Free convection in a complex enclosure: Heatline and Entropy generation study

Rujda Parveen

Department of Mathematics, Visva-Bharati (A Central University),

Santiniketan - 731 235, West-Bengal, India.

Abstract

Numerical study of heat transfer characteristics due to steady laminar free convection within an enclosure with curved upper wall has been investigated. The bottom wall is considered to be uniformly heated, while the two side walls are linearly heated and the upper curved wall is adiabatic. The test has been performed for wide range of governing parameters like Prandtl number ($Pr = 0.7$ and 1000), Rayleigh number ($10^3 \leq Ra \leq 10^5$) and various concavity and convexity of the upper wall in order to examine the heat transfer and change in motion of fluid flow within the enclosure. Numerical simulations are presented in terms of streamlines (ψ), isotherms (θ), heat transfer irreversibility (S_θ), fluid friction irreversibility (S_ψ), heatlines (Π), average Nusselt number ($\overline{Nu}$) and average Bejan number (Be_{avg}). The present study shows that the change in curvature of the upper wall affects the thermal behaviour of the fluid inside the enclosure. It is observed that the heat transmission rate in highly convex domain is more as compared to concave domains.

Keywords: free convection flow; Complex enclosure; Entropy generation; Heatline; Nusselt number.

1   Introduction

Free convection or natural convection inside an enclosure or closed cavities has been studied predominantly due to its substantial attention in nature and energy related applications such as solar collector, cooling of electronic components, geothermal energy system, designing of building, food processing etc.

1

Several investigation on natural convection had been conducted on enclosures with regular geometries (square, rectangular, triangular, trapezoidal etc.) as the thermal characteristics are less complex than the irregular enclosures. Davis [1] considered a square-shaped cavity with differentially heated side walls to study natural convection. Basak et al. [3] investigated the free convection inside a square cavity with uniformly and non uniformly heated bottom wall. He observed that the heat transfer is greater in case of non uniform heating as compared to uniform heating case. Kimura and Bejan [4] provided a heatline visualization method for heat transfer in a square cavity. Saha and Khan [5] performed a review study on the free convection heat transfer in an attic-shaped space. Natural convection in enclosure having triangular shapes has been studied by Kent et al. [6,7]. Free convection experiments have also been conducted in trapezoidal enclosures by researchers. Moukalled and Darwish [8] investigated the influence of the baffle height and position on the upper inclined surface of a trapezoidal enclosure. It was found that the overall heat transfer rate is highly effected by the presence of the baffle. Ramakrishna et al. [9] have studied entropy generation and heatlines for free convection in a trapezoidal cavity where left wall is hot and right wall is maintained at constant cold temperature while the horizontal walls are adiabatic.

Studies dealing with convection problems inside complicated geometries are limited because of complexity of flow inside enclosure which significantly affects the thermal behavior of the fluid inside it. Application of such curved and wavy enclosures is often used in solar energy system, electric machinery, microelectronic industries etc. Morsi and Das [10] numerically found the heat transfer characteristics and flow patterns for complex enclosure. Varol and oztop [11] conducted expriment to find the effects of aspect ratio on the free convection heat transfer in a tilted solar collector having absorber on the wavy bottom surface. They observed that the aspect ratio is an effective parameter which can be used to control the heat transfer inside the collector. Das and Mahmud [12] numerically investigated thermal behaviour of fluid inside an enclosure consisting of horizontal wavy wall and vertical straight wall. They obtained that when the amplitude-wavelength ratio changes from zero to other values at lower Grashoff number, heat transfer rate rises. Mahmud and Islam [13] carried out laminar free convection and entropy generation inside an inclined wavy enclosure. They indicated that, lower the surface waviness, higher is the heat transfer for a particular angular position. Dalal and Das [14,15] have considered

an enclosure with a wavy vertical wall to analyze free convection. They obtained that the undulation in the right wall effects the flow field, thermal field and heatlines. In a differentially heated inclined square chamber with various undulations, Adjlout et al. [16] investigated the impact of a hot wavy wall caused by laminar natural convection.

Based on the above wide literature survey, it is found that study of heat transfer characteristics in complex geometries is essential in order to obtain the optimal design of the container for various industrial applications. The main interest of this investigation is to study the effect of change in amplitude in the distribution of heat and fluid flow due to free convection inside an enclosure having a top adiabatic curved wall, linearly heated side walls and uniformly heated bottom wall. In the present chapter, the effects of Rayleigh number, Prandtl number and amplitude of the upper wall are investigated simultaneously to understand the importance of these parameters on the characteristics of free convection.. Results are presented in terms of isotherms (θ), streamlines (ψ), heat transfer irreversibility (S_θ), fluid friction irreversibility (S_ψ) and heatlines (Π). The influence of Ra and h on the average Bejan number and average Nusselt number is also shown. To solve the non-linear coupled partial differential equations in the current work, the Bi-Conjugate Gradient Stabilized technique (BiCGStab) is used.

2 Mathematical formulations

3 Physical model

For the present problem, we have considered a modified square enclosure of length L with convex or concave upper wall whose amplitude is H. The dimensionless function F(X) which represents the shape of the curved wall of the enclosure is given by

$$F(X) = 1 + h sin(\pi X)$$

where h (=H/L) is the amplitude of the upper wall. When h is positive, upper wall is concave but when h is negative, upper wall is convex. Fig. 1 shows the physical domain of differentially heated enclosure with concave (a) and convex (c) top wall and computational domain (b).
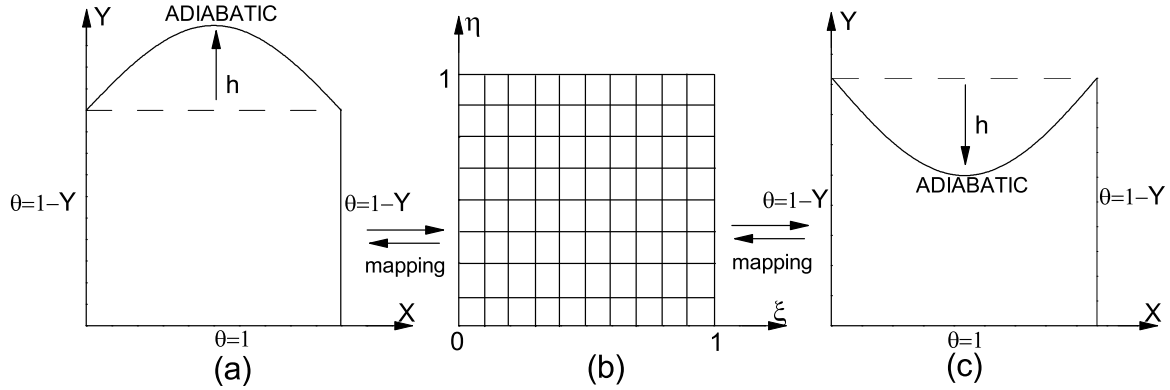
Fig. 1: Diagram of the physical domain (a,c) and computational domain (b) with boundary conditions.

The left and right walls are linearly heated , the bottom wall is uniformly heated and the top curved wall is kept adiabatic. The flow is steady, 2-D, laminar and incompressible.

3.1 *Governing equations*

The governing equations in non-dimensional form for the present problem can be written as:

$$U_X + V_Y = 0 \tag{1}$$

$$UU_X + VU_Y = -P_X + Pr(U_{XX} + U_{YY}) \tag{2}$$

$$UV_X + VV_Y = -P_Y + Pr(V_{XX} + V_{YY}) + RaPr\theta \tag{3}$$

$$U\theta_X + V\theta_Y = \theta_{XX} + \theta_{YY} \tag{4}$$

where X and Y are non-dimensional coordinates along horizontal and vertical directions respectively, U and V are non-dimensional velocity components in X and Y directions respectively, P is the dimensionless pressure, θ is the dimensionless temperature, Ra and Pr are the Rayleigh number and Prandtl number respectively.

4

The dimensionless parameters in the above equations are defined as follows

$$(X, Y) = \frac{x, y}{L}, \ U = \frac{uL}{\alpha}, \ V = \frac{vL}{\alpha}, \ P = \frac{pL^2}{\rho\alpha^2},$$

$$\theta = \frac{T - T_c}{T_h - T_c}, \ Pr = \frac{\nu}{\alpha}, \ Ra = \frac{g\beta(T_h - T_c)L^3}{\nu\alpha}$$

where x and y are distances along the horizontal and vertical directions respectively, u and v are the velocity components in the x and y directions respectively, $\alpha, \beta, \nu, \rho, g, T_h, T_c$ are thermal diffusivity, coefficient of volumetric expansion, kinematic viscosity, density of the fluid, gravitational acceleration, temperature of the bottom wall and temperature of top-left / top-right corner, respectively. Stream function (ψ) and vorticity (ω) are defined as

$$U = \psi_Y, \quad V = -\psi_X, \quad \omega = V_X - U_Y. \tag{5}$$

The anticlockwise circulation is denoted by positive sign and clockwise circulation is represented by negative sign.

3.2   *Boundary conditions*

The corresponding dimensionless boundary conditions for the present problem are specified as follows: All walls, $U = 0$, $V = 0$, $\psi = 0$
At bottom wall, $\theta = 1$
At left and right vertical walls, $\theta = 1 - Y$
At top curved wall, $\frac{\partial \theta}{\partial Y} = 0$

3.3   *Nusselt number*

The Nusselt number, Nu is the measure of convective heat transfer coefficient at the hot surface. Higher the value of Nu, higher is the heat transfer rate from the surface.
The local Nusselt number is computed as

$$Nu = -\frac{\partial \theta}{\partial n},$$

where n denotes the direction of normal to the plane.
The local Nusselt number along the left wall (Nu_l), right wall (Nu_r) and bottom wall

(Nu_b) are defined as follows,

$$Nu_l = \theta_X, \quad Nu_r = -\theta_X, \quad Nu_b = \theta_Y$$

The average Nusselt number is obtained by integrating the local Nusselt number along the respective wall. The average Nusselt number along left wall, right wall and bottom wall are given by

$$\overline{Nu_l} = \int_0^1 Nu_l dX, \quad \overline{Nu_r} = \int_0^1 Nu_r dX, \quad \overline{Nu_b} = \int_0^1 Nu_b dY. \tag{6}$$

To evaluate eq. (6), a Simpson's $\frac{1}{3}$rd rule of integration is implemented.

3.4 *Entropy generation*

The dimensionless local entropy production due to heat transfer (S_θ) and due to fluid friction (S_ψ) for a two-dimensional heat and fluid flow in the cartesian coordinate can be expressed as follows:

$$
\begin{aligned}
S_\theta &= (\theta_X)^2 + (\theta_Y)^2, \\
S_\psi &= \phi \left[2 \left((U_X)^2 + (V_Y)^2 \right) + (U_Y + V_X)^2 \right]
\end{aligned}
$$

where ϕ is the irreversibility ratio, defined as

$$\phi = \frac{\mu T_0}{k} \left(\frac{\alpha}{L\Delta T} \right)^2$$

μ and k being dynamic viscosity and thermal conductivity of the fluid respectively. Here, we have considered ϕ as 10^{-4}.

The local entropy generation S_l is the sum of S_θ and S_ψ:

$$S_l = S_\theta + S_\psi \tag{7}$$

The total entropy generation due to heat transfer to $(S_{t\theta})$ and due to fluid friction $S_{t\psi}$ are obtained by integrating the local entropy generation by the system volume

$$
\begin{aligned}
S_{t\theta} &= \int_V S_\theta dV \\
S_{t\psi} &= \int_V S_\psi dV \\
S_{total} &= S_{t\theta} + S_{t\psi}
\end{aligned}
$$

6

The average Bejan number indicates the strength of the entropy generation due to heat transfer irreversibility and is defined as the ratio of heat transfer irreversibility to total entropy generation

$$Be_{avg} = \frac{S_{t\theta}}{S_{t\theta} + S_{t\psi}} = \frac{S_{t\theta}}{S_{total}}$$

If $Be_{avg} > \frac{1}{2}$, the heat transfer irreversibility is dominating, while if $Be_{avg} < \frac{1}{2}$, the irreversibility due to fluid friction dominates the process and if $Be_{avg} = \frac{1}{2}$, the entropy generation due to viscous effects and heat transfer are equal.

3.5 *Heat function*

Similar to streamlines, the heatline can be used to show the direction and intensity of heat flow. The heat function Pi produced from conductive heat fluxes $(-\theta_X, -\theta_Y)$ and convective heat fluxes $(U\theta, V\theta)$ is used to depict the heatflow within the enclosure. The dimensionless form of heat function for a two dimensional convective problem can be obtained from

$$\begin{aligned} \Pi_Y &= U\theta - \theta_X \\ -\Pi_X &= V\theta - \theta_Y \end{aligned}$$

which are derived from eqs. (1) and (4).

The above eqs. lead to the following differential equation for heat function

$$\Pi_{XX} + \Pi_{YY} = (U\theta)_Y - (V\theta)_X \tag{8}$$

where Π is dimensionless heat function. We consider that Π is a continuous function with continuous second order partial derivatives.

The boundary conditions for Π are specified as follows:

At bottom wall, $n.\nabla\Pi = 0$,

At left wall, $n.\nabla\Pi = 1$,

At right wall, $n.\nabla\Pi = -1$,

At top curved wall, $\Pi = 0$

The following Dirichlet's conditions are used:

At bottom left corner $\Pi = \overline{Nu_l}$,

At bottom right corner $\Pi = -\overline{Nu_r}$

where $\overline{Nu_l}$ and $\overline{Nu_r}$ are average Nusselt number at left and right wall respectively.

4   Numerical Procedure

Eliminating the pressure term from eq.(2) and (3) and rewriting the equation of conservation of mass, momentum in terms of stream function (ψ) and vorticity (ω), we get

$$\psi_{XX} + \psi_{YY} = -\omega, \tag{9}$$

$$Pr\left(\omega_{XX} + \omega_{YY}\partial Y^2\right) - (U\omega_X + V\omega_Y) + RaPr\theta_X = 0, \tag{10}$$

where

$$U = \psi_Y, \quad V = -\psi_X.$$

The irregular physical domain (X, Y) is transformed and converted into a computational domain (square) using coordinate transformation:

$$\xi = X \quad \eta = Y/(1 + h\sin\pi X)$$

The above transformation transforms the curved upper boundary $Y = F(X)$ into the straight line $\eta = 1$.

The governing equations are evaluated in $\xi - \eta$ domain using the relationship:

$$\begin{pmatrix} \xi_X & \xi_Y \\ \eta_X & \eta_Y \end{pmatrix} = \frac{1}{J} \begin{pmatrix} Y_\eta & -X_\eta \\ -Y_\xi & X_\xi \end{pmatrix}$$

where,

$$J = \frac{\partial(X, Y)}{\partial(\xi, \eta)} = \begin{vmatrix} X_\xi & X_\eta \\ Y_\xi & Y_\eta \end{vmatrix}.$$

It is difficult to solve the problem analytically due to the existence of non-linear terms in the governing Eqs. (1-4). Using the aforesaid transformation, the equations are changed into a bi-harmonic equation in the stream function-velocity formulation which are discretized further using a finite difference scheme. An outer-inner iteration procedure,

biconjugate gradient stabilized method (BiCGStab) is employed to solve the discretized set of equations. The tri diagonal system

$$(\psi_\xi)_{i+1,j} + 4\,(\psi_\xi)_{i,j} + (\psi_\xi)_{i-1,j} \quad = \quad \frac{3}{d}(\psi_{i+1,j} - \psi_{i-1,j}), \tag{11}$$

$$(\psi_\eta)_{i,j+1} + 4\,(\psi_\eta)_{i,j} + (\psi_\eta)_{i,j-1} \quad = \quad \frac{3}{d}(\psi_{i,j+1} - \psi_{i,j-1}). \tag{12}$$

is solved by using Thomas algorithm to get ψ_ξ and ψ_η (d is the step length on a uniform rectangular mesh). The computed ψ_ξ and ψ_η values are then used to derive velocity values, u* and v*. More details of the used numerical scheme are presented in [17]. The cycle of numerical iteration continues until the convergence criterion (0.5×10^{-6}) is satisfied. The graphical presentation of this study has been performed by using GNUPLOT.

5   Results and discussion

In this section, numerical studies of flow and heat transfer in a complex enclosure are discussed. Computations are performed for various Rayleigh number $(Ra = 10^3 - 10^5)$, Prandtl number $(Pr = 0.7$ and $1000)$ with various amplitude (h) of top wall. Five different shapes of top wall are considered to study the curvature effect on fluid flow and heat flow distribution. The original square enclosure is modified into a complex enclosure by changing the curvature of the top wall. Figs. 3-6 represent the isotherms (θ),streamlines (ψ), heat transfer irreversibility (S_θ), fluid friction irreversibility (S_ψ) and heatlines (Π) for different values Pr, Ra and h.

5.1   Streamlines and isotherms

It is clear from Fig. 2 that at low $Ra = 10^3$ the buoyancy effect is weak and heat transfer is primarily due to conduction. Isotherm lines are smooth, uniform and parallel near the uniformly heated bottom wall and follow the geometry of wavy surface. For square enclosures $(h = 0)$, isotherms with $\theta \geq 0.4$ are smooth curves which span the entire enclosure and with $\theta \leq 0.3$, the isotherms occur symmetrically near the top corners of the linearly heated side walls. As the concavity increases, the qualitative trends of isotherms remains almost similar to square enclosure while as convexity increases the isotherms are found to be compressed at the corner regions due to less availability of area signifying higher
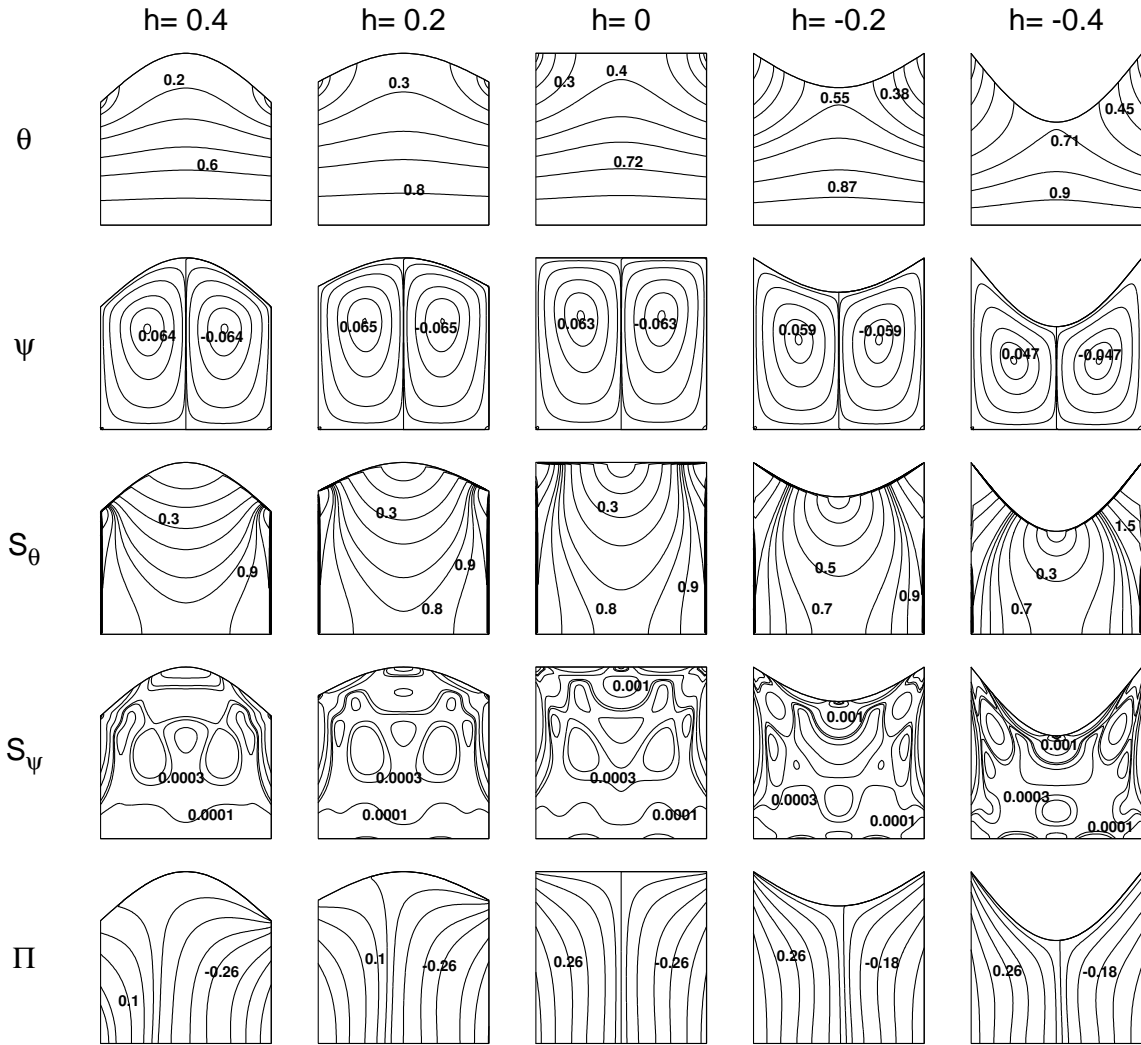
Fig. 2: Isotherms (θ), streamlines (ψ), heat transfer irreversibility (S_θ), fluid friction irreversibility (S_ψ) and heatlines (Π) for $Pr = 0.7$ and $Ra = 10^3$.

heat transfer rate. Because of temperature difference, the fluid moves upward from the middle portion of the bottom wall towards the crest of the cavity and falls along the side walls forming two symmetric counter-rotating circulations having the same strength with respect to the centerline of the cavity. As Ra is low, the circulation is weak due to less prominent convection (see Fig. 2). It is found that $|\psi|_{max} = 0.063$ for square enclosure. As the concavity of the top wall increases, slight increase in the magnitude of $|\psi|_{max}$ is observed which in contrast significantly decreases as the convexity increases.

As Ra increases to 10^4, the isothermal lines swirl due to the influence of convection current for all h (Fig. 3). Also the buoyancy effect increases which results in expansion of vortices and becomes dense. The intensity of fluid flow increases to $|\psi|_{max} = 1.69$ for $h = 0$ as compared to the case of $Ra = 10^3$. Further $|\psi|_{max}$ increases or decreases on increasing the concavity and convexity respectively (Fig. 3).

Beyond $Ra = 10^4$, the effect of viscous force becomes weak and thermal force plays a dominant role. Significant distortion of the isotherms occur within the enclosures because of high convection. On increasing concavity isotherms are found to be highly distorted whereas highly compressed isotherms are observed as the convexity increases enhancing higher heat transfer rate. In other words, the heat transfer is dominated by convection rather than conduction under high Ra. Multiple circulations are observed in square enclosure with greater magnitude $|\psi|_{max} = 6.6$ at $Ra = 10^5$. As h increases the intensity of primary as well as secondary circulation increases. In the reverse scenario the multicellular flow patterns turns into a bicellular flow pattern with the increase of convexity. (Fig. 4).

Because of high momentum diffusivity at $Pr = 1000$ and $Ra = 10^5$, the isotherms get further compressed along the lower and side wall in square enclosure (Fig. 5). On increasing concavity of the top wall, the isotherms starts getting deformed because of enhanced convection. As the buoyancy force starts dominating the viscous force at high Ra and hence the isotherms are unable to maintain the smoothness and dispersed throughout the enclosure. Significantly stronger intensity of fluid circulations can be seen from Fig. 5 which shows $|\psi|_{max} = 11.1$ for square enclosure. The increase in magnitude of $|\psi|_{max}$ illustrates that convection strength increases with high Pr. The primary fluid circulation vortices grow bigger in size and occupy almost the entire part of the enclosure. However, the secondary vortices are found near the corners of the bottom wall. It is also observed

that the fluid takes the shape of the cavity for higher Pr that signifies thermal mixing. Reasonable changes are observed on increasing concavity of top wall. The two symmetric primary vortices in square enclosure splits into multiple vortex, one large dominated vortex diagonally elongated and secondary vortices appear above and below the diagonal vortex (Fig. 5). The two inner vortices are merged with each other in an elongated vortex. On increasing the convexity of the top wall, the secondary circulations are squeezed and begin to disappear and symmetric eddies are observed with decrease in magnitude of $|\psi|_{max}$ because of high convection effect.

5.2   Entropy generation

Fig. 2 shows that due to high thermal gradient between the top wall and side wall, the maximum value of S_θ ($S_{\theta,max} = 17.42$) occurs at the top corners for square enclosure. The values of S_θ are very low at the central zone of the enclosure due to low temperature gradient. As h increases from zero to positive values the isotherms get dispersed resulting in less thermal gradient and the value of $S_{\theta,max}$ decreases, whereas when h decreases from zero, largely compressed isotherms are observed near the side and top wall which results in increasing temperature gradient and consequently $S_{\theta,max}$ increases (see Table 3). Table 4 shows the maximum values of S_ψ for various values of Pr, Ra and h. It is clear from this table that as the fluid circulation cells are weak at low Ra, thus S_ψ is insignificant relative to S_θ with $S_{\psi,max} = 0.008$ for square enclosure. From Fig. 3 it is observed that the effect of S_ψ is significant at the corners of the curved wall of the enclosure because of velocity gradient between the cavity wall and adjacent flow circulation cell, while S_ψ is almost negligible at the core. Thus S_θ dominates S_ψ at low Ra, for all cases.

As Ra increases to 10^4, isotherms are found to be highly compressed due to enhanced convection, resulting in large $S_{\theta,max} = 25.29$ compared to the case of $Ra = 10^3$ for square enclosure (Fig. 3). As concavity increases more circular loops are observed due to which the heat transfer and $S_{\theta,max}$ decreases. Further it is observed that as convexity increases the circular loops dissolve indicating higher $S_{\theta,max}$ at the corner regions of the curved wall. Also high $S_{\psi,max} = 3.87$ for $h = 0$ is noticed because of increase in fluid flow and large velocity gradient. From Table 4, it can be seen that the convex cases exhibit lesser $S_{\psi,max}$ as compared to concave cases.
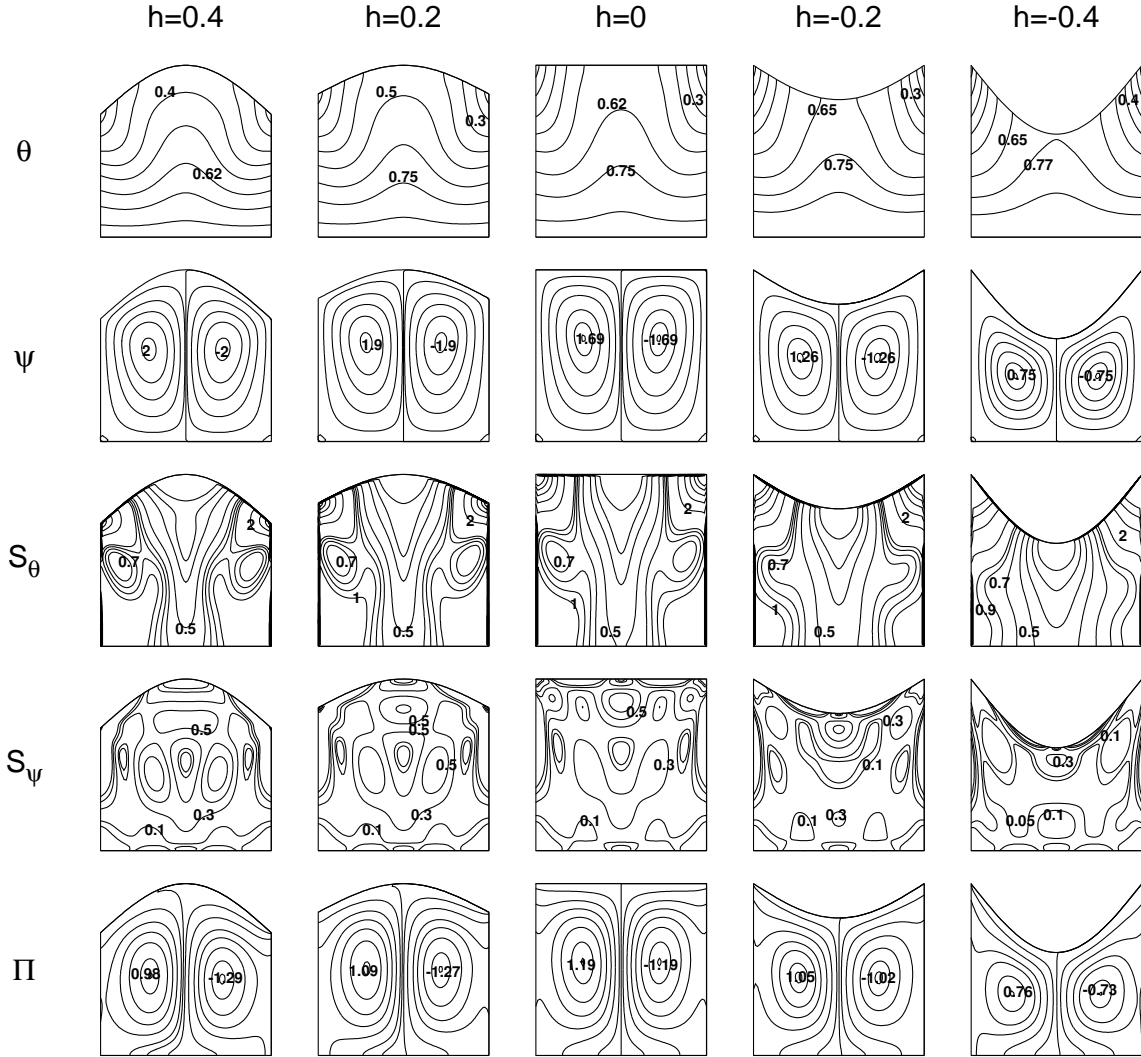
12

Fig. 3: Isotherms (θ), streamlines (ψ), heat transfer irreversibility (S_θ), fluid friction irreversibility (S_ψ) and heatlines (Π) for $Pr = 0.7$ and $Ra = 10^4$.

13

S_θ is significant for $Ra = 10^5$ due to high convection effect. Large compression of isotherms results in large $S_{\theta,max} = 43.92$ for square enclosure (see Fig. 4). The contours of S_θ at the core region are similar for all the cases ($S_\theta = 0.1$) due to less temperature gradient in this region. Because of high intensity of fluid circulation at $Ra = 10^5$, the velocity gradient are larger compared to temperature gradient resulting in larger $S_{\psi,max}$ for all h, see Table 4. An increase in concavity improves buoyancy and consequently the fluid flow effect which results in high S_ψ. Overall, it is observed that due to the presence of high convective effect at high Ra, the velocity gradient increases. Thus S_ψ dominates over S_θ throughout the cavity for all cases.

Maximum entropy generation due to heat transfer is observed for $Pr = 1000$ and $Ra = 10^5$ because of high temperature gradient. The isotherms are found to be strongly compressed as compared to $Pr = 0.7$ (Fig. 6). It is obtained that $S_{\theta,max} = 80.21$ for square enclosure. Strong convection induces greater buoyancy effect for high Pr. Similar to lower Pr, the value of $S_{\theta,max}$ for concave cases are less as compared to the convex cases due to highly compressed isotherms at the corner regions of the curved walls. Also the value of $S_{\psi,max}$ are larger for concave cases than those of convex cases (Table 4). The presence of intense streamline cells at $h = 0.2$ results in high velocity gradients causing higher value of $S_{\psi,max}$. S_ψ is almost similar at the interior region for all the cases. Comparatively larger values of $S_{\psi,max}$ are observed than those of $S_{\theta,max}$ throughout the enclosure.

Table 1: Values of $S_{\theta,max}$ at $Pr = 0.7$ and 1000 for $Ra = 10^3 - 10^5$ with various amplitude of upper wall (h).

h	$Pr = 0.7$			$Pr = 1000$		
	$Ra = 10^3$	$Ra = 10^4$	$Ra = 10^5$	$Ra = 10^3$	$Ra = 10^4$	$Ra = 10^5$
-0.4	64.58	69.63	101.65	64.58	69.54	109.03
-0.2	33.27	40.36	66.35	33.27	31.52	85.75
0	17.42	25.29	43.92	17.42	25.71	80.21
0.2	12.00	19.06	39.72	12.00	22.12	74.52
0.4	11.23	16.69	34.05	11.23	17.87	49.14

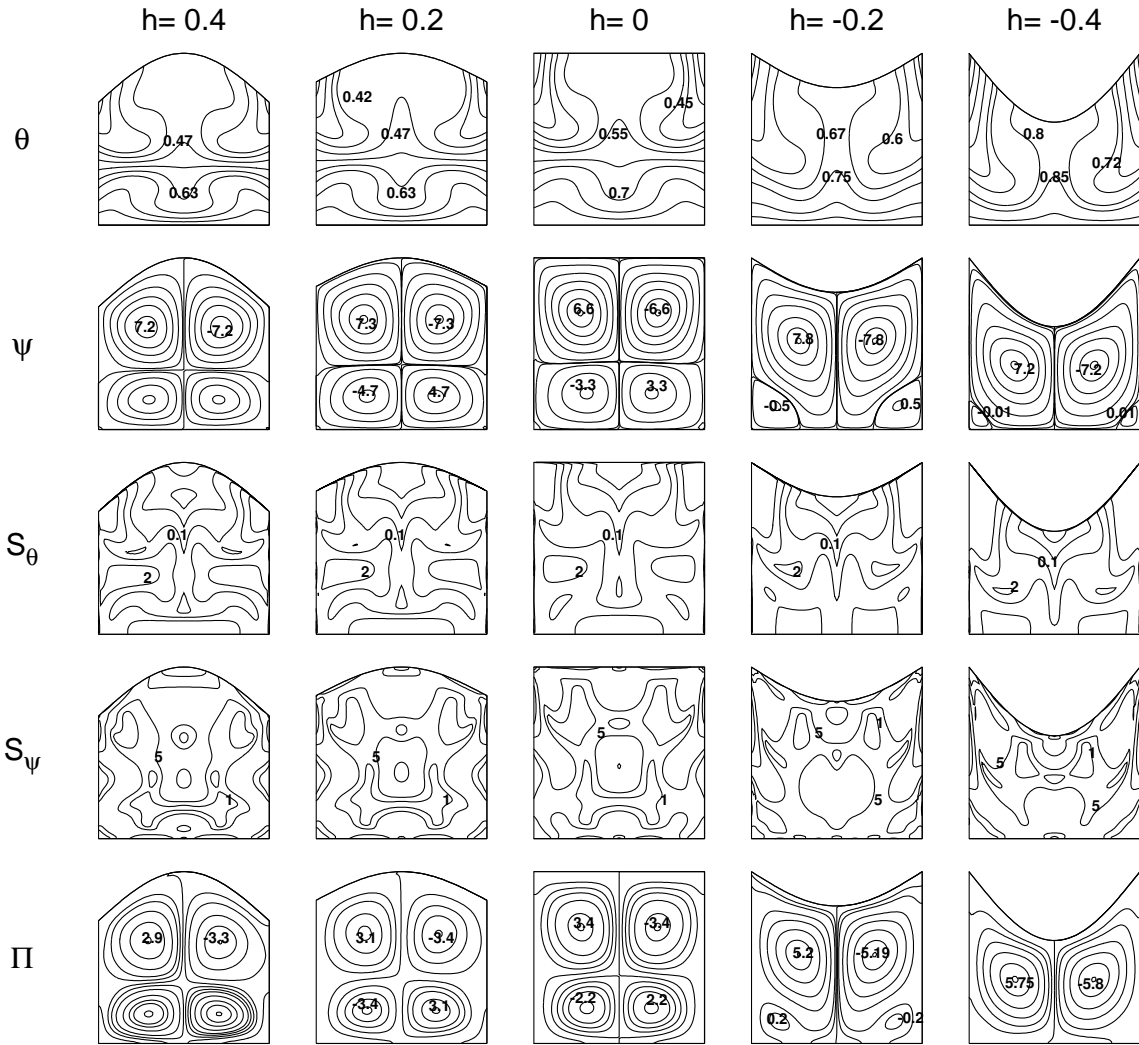Fig. 4: Isotherms (θ), streamlines (ψ), entropy generation due to heat transfer (S_θ), entropy generation due to fluid friction (S_ψ) and heatlines (Π) for $Pr = 0.7$ and $Ra = 10^5$.

Table 2: Values of $S_{\theta,max}$ at $Pr = 0.7$ and 1000 for $Ra = 10^3 - 10^5$ with various amplitude of upper wall (h).

h	$Pr = 0.7$			$Pr = 1000$		
	$Ra = 10^3$	$Ra = 10^4$	$Ra = 10^5$	$Ra = 10^3$	$Ra = 10^4$	$Ra = 10^5$
-0.4	0.0076	1.39	237.55	0.0069	1.29	202.20
-0.2	0.0074	2.45	251.19	0.0073	2.83	291.84
0	0.0088	3.87	191.24	0.0071	3.54	359.82
0.2	0.0069	4.79	210.55	0.0072	4.19	375.30
0.4	0.0035	4.99	202	0.0077	5.74	296.18

5.3 Heatlines

Heatlines are used to depict the direction of heat movement. In Fig. 2, end-to-end heatlines joining the bottom wall and surrounding side walls are seen at low Ra.. In this figure heatlines are smooth and symmetrical with respect to middle line for square enclosure depicting high conductive heat transfer. At the top of the side walls, there are intense heatlines. It is found that $|\Pi|_{max} = 0.46$ for $h = 0$ (Fig. 2). As the concavity grows, asymmetric heatlines are seen that are dense in the top portion of the right wall as compared to the left wall, and as a result, the value of $|Pi|max$ declines. However, as convexity increases, dense heatlines may be seen at the higher portion of the left wall relative to the right wall, which causes the value of $|\Pi|_{max}$to rise.

Interesting features are observed for $Ra = 10^4$ in Fig. 3. The straight heatlines are transformed to two symmetric eddies in the whole region of the enclosure due to convection dominant heat transfer. Intense vertical heatlines are observed at the core and near the side walls (Fig. 3). Similar to low Ra dense heatlines are formed in the right wall as h increases and in left wall as h decreases.

As $Ra = 10^5$, similar to streamline, symmetric primary heatline circulations are observed in the top portion and secondary circulations span near the lower half. Due to enhanced thermal mixing, higher intensity of closed loop heatlines are observed at the core. With the increase of Ra magnitude of heatfunction increases which implies that the amount of heat transfer rate is higher. The intensity of primary circulations are higher as compared to lower secondary circulations. As h decreases from 0 to -0.4, the secondary circulations

begin to vanish and large symmetric primary circulations are found to span and take the shape of the enclosure. As a result heatlines are closely compact depicting higher heat transfer gradient. However as h increase from 0 to 0.4, intensity of primary circulation decreases and secondary circulation increases (Fig. 4).

For high $Pr = 1000$, $Ra = 10^5$, due to enhanced thermal mixing, two symmetric primary eddies are observed in square enclosure of high intensity and compressed secondary circulations of lower intensity near the bottom wall are formed. Magnitude of $|\Pi|_{max}$ is larger compared to low $Pr = 0.7$. As the concavity increases, the secondary eddies start to grow and at $h = 0.4$ large diagonally elongated eddies are formed having secondary eddies above and below the elongated eddies. While the secondary eddies begin to vanish as h decreases. (see Fig. 5)

5.4 Nusselt number and Bejan's number

Fig. 6 shows the effect of various curvature of the upper wall on average Nusselt number ($\overline{Nu}$) and average Bejan's number (Be_{avg}) for different Rayleigh number ($10^3 - 10^5$) at $Pr = 0.7$ and 1000.

Heat transfer is mainly due to conduction at low $Ra = 10^3$. As the convective mode of heat transfer becomes dominant with the increase of Ra, there is an increase in $\overline{Nu}$ for all values of h causing a high heat transfer effect within the enclosure. It is clear from Fig. 7 ((a) and (c)), the rate of heat transfer increases as h decreases when Ra and Pr are kept fixed. The $\overline{Nu}$ even becomes negative for $h = 0.4$ depicting that the heat generated in the bottom wall cannot be transferred to the top wall. This shows that $\overline{Nu}$ is larger in highly convex case ($h = -0.4$) as compared to other cases. Similar trend is observed at high $Pr = 1000$. Because of large momentum diffusivity at high Pr, $\overline{Nu}$ is significantly larger than that of $Pr = 0.7$ for all h.

At low $Ra = 10^3$, $Be_{avg} \cong 1$ for all values of h, because entropy generation due to heat transfer irreversibility is high compared to irreversibility effect caused by the fluid friction. As Ra increases, convection heat transfer becomes dominant, the effect of viscosity flow on entropy generation becomes stronger that leads to decrease in Be_{avg}. As h increases from 0 to 0.4, $S_{\theta,max}$ is larger than $S_{\psi,max}$ at $Ra = 10^3$. Whereas, as h decreases from 0 to -0.4 compressed isotherms are observed that results in increase in $S_{\theta,max}$ at $Ra = 10^5$
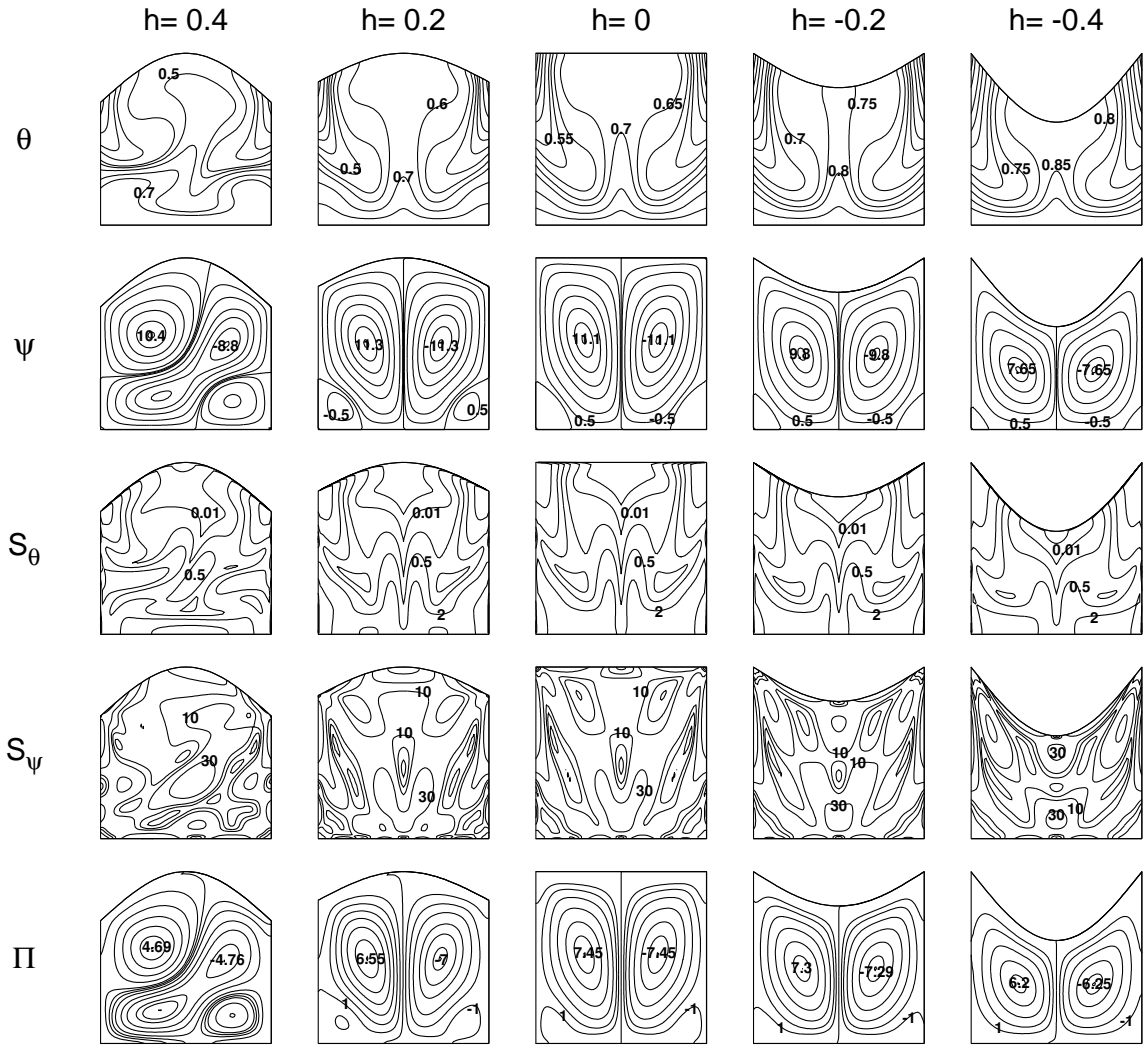
Fig. 5: Isotherms (θ), streamlines (ψ), heat transfer irreversibility (S_θ), fluid friction irreversibility (S_ψ) and heatlines (Π) for $Pr = 1000$ and $Ra = 10^5$.
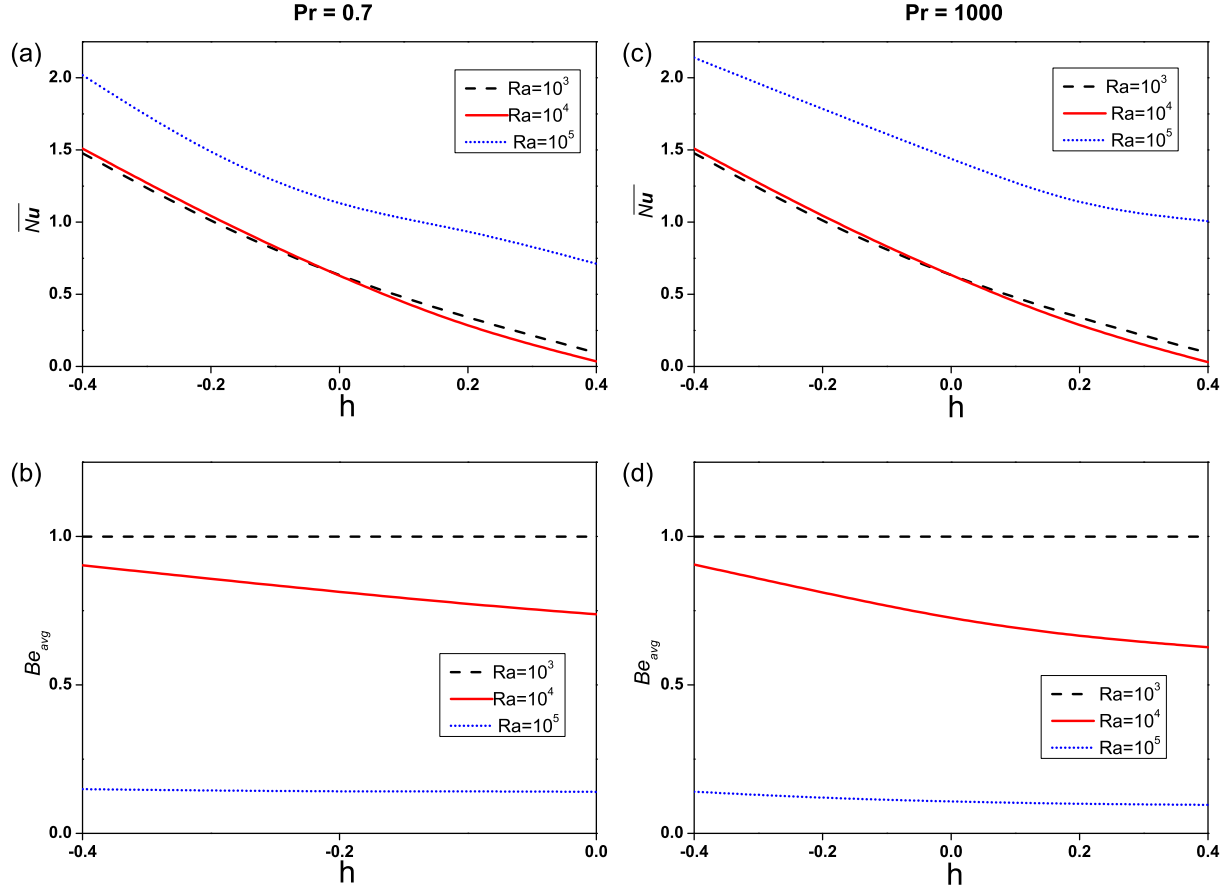
Fig. 6: Variation of average Nusselt number ($\overline{Nu}$) and average Bejan number (Be_{avg}) with h for various curvature at $Pr = 0.7$ and 1000.

and consequently Be_{avg} increases (Fig. 6 ((b) and (d))). As Pr increases from 0.7 to 1000, Be_{avg} decreases due to high momentum diffusivity and rapid increase in magnitude of $S_{\psi,max}$ for all cases. Qualitative distribution of $\overline{Nu}$ and Be_{avg} are similar for $Pr = 0.7$ and 1000.

Overall it is observed that $Be_{avg} > \frac{1}{2}$ for low Ra which shows that heat transfer irreversibility is dominant in the enclosure while for high Ra, $Be_{avg} < \frac{1}{2}$ depicting that heat transfer irreversibility due to fluid friction becomes dominant.

6 Conclusion

Study of free convection in a complex enclosure has been investigated numerically. The thermal flow characteristics are obtained for various Rayleigh number $(10^3 - 10^5)$ and $Pr = 0.7$ and 1000. The main conclusions drawn from the present study are as follows:

1. At low Ra, the heat transfer is due to conduction hence smooth isotherms are observed. The isotherms gets more compressed with the increase of Ra and Pr due to enhanced convection. Heat transfer rate is found to be more in convex cases as compared to concave cases.

2. The intensity and magnitude of streamlines increases with the increase of Ra and Pr. Multiple vortices are observed at $Ra = 10^5$. $|\psi|_{max}$ increases with the increase of h and decreases with the decrease of h.

3. $S_{\theta,max}$ increases with increase of Ra and Pr due to enhanced convection. Comparative studies show that $S_{\theta,max}$ is highest in convex cases and least in concave cases or all Ra and Pr.

4. $S_{\psi,max}$ is found to be very less at low Ra, which increases with the increase of Ra and Pr. As the fluid flow effect improves with increasing h, $S_{\psi,max}$ is found to be more in concave cases compared to convex cases.

5. Heatline contours are almost similar to streamlines. The intensity of heatline increases with the increase of Ra and Pr because of increase of convection. Dense heatlines are observed with the increase of h resulting in high magnitude of heatfunction whereas heatlines are found to be segregated as h decreases and the magnitude of heatfunction decreases.

6. $\overline{Nu}$ increase with the increase of Ra and Pr. As the heat transfer rate is found to be higher in convex cases as compared to concave cases, $\overline{Nu}$ increases when h decreases from 0 to -0.4 and decreases when h increases from 0 to 0.4.

7. At low Ra, $Be_{avg} > \frac{1}{2}$ which signifies that entropy generation in the enclosure is mainly due to heat transfer irreversibility. With the increase of Ra, buoyancy force becomes dominant which results in increase in entropy generation due to fluid friction irreversibility, consequently $Be_{avg} < \frac{1}{2}$.

References

[1] G.de Vahl Davis, Natural convection of air in a square cavity: a benchmark numerical solution, Int. J. Numerical Methods in fluids 3 (1983) 249-264.

[2] Q.H. Deng, G.F. Tang, Numerical visualization of mass and heat transport for conjugate natural convection/heat conduction by streamline and heatline, Int. J. Heat Mass Transfer 45 (2002) 2373-2385.

[3] T. Basak, S. Roy, A.R. Balakrishnan Effects of thermal boundary conditions on natural convection flows within a square cavity, Int. J. Heat Mass Transfer 49 (2006) 4525-4535.

[4] S. Kimura, A. Bejan, The Heatline visualization of convective heat transfer, J. Heat Transfer 105 (1983) 916-919.

[5] S.C. Saha, M.M.K. Khan, A review of natural convection and heat transfer in attic-shaped space, Energy and Buildings 43 (2011) 2564-2571.

[6] E.Faud Kent, Numerical analysis of laminar natural convection in isosceles triangular enclosure for cold base and hot inclined walls, Mechanics Research Comm. 36 (2009) 497-508.

[7] E.Faud Kent, E. Asmaz, S. Ozerbay, Laminar natural convection in right triangular enclosures, Heat Mass Transfer 44 (2007) 187-200.

[8] F. Moukalled, M. Darwish, Natural convection in a trapezoidal enclosure heated from the side with a baffle mounted on its upper inclined surface, Heat Tranfer Engg. 25 (8) (2004) 80-93.

[9] D. Ramakrishna, T. Basak, S. Roy, Analysis of heatlines and entropy generation during free convection within trapezoidal cavities. Int. Comm. in Heat Mass Transfer 45 (2013) 32-40.

[10] Y.S. Morsi, S. Das, Numerical Investigation of Natural Convection inside Complex Enclosures, Heat Transfer Engg. 24 (2) (2003) 30-41.

[11] Y. Varol, H.F. Öztop, Buoyancy induced heat transfer and fluid flow inside a tilted wavy solar collector, Building and Environment 42 (2007), 2062-2071.

[12] P.K. Das, S. Mahmud, Numerical investigation of natural convection inside a wavy enclosure, Int. J. Therm. Sci. 42 (2003) 397-406.

[13] S. Mahmud, A.K.M. Sadrul Islam, Laminar free convection and entropy generation inside an inclined wavy enclosure, Int. J. Therm. Sci. 42 (2003) 1003-1012.

[14] A. Dalal, M.K. Das, Natural Convection in a Cavity With a Wavy Wall Heated From Below and Uniformly Cooled From the Top and Both Sides, J. of Heat Transfer 128 (7) (2006) 717-725.

[15] A. Dalal, M.K. Das, Heatline method of visualization of natural convection in a complicated cavity, Int. J. Heat Mass Transfer 5 1(2008) 263-272.

[16] L. Adjoult, O. Imine, A. Azzi, M. Belkadi, Laminar natural convection in an inclined cavity with a wavy wall, Int. J. Heat Mass Transfer 45 (2002) 2141-2152.

[17] R. Parveen, T.R. Mahapatra, Numerical simulation of MHD double diffusive natural convection and entropy generation in a wavy enclosure filled with nanofluid with discrete heating, Heliyon 5 (2019) e02496.